CASCADE Open Aircraft Project: University of Bristol VTOL Drone Development

Thomas David* Duncan Hine† Ben Schellenberg‡ Hirad Goudarzi§ Tom Rendall¶ Kieran Wood‖ Joaquim Bolós-Fernández** Tom Richardson††
University of Bristol, United Kingdom

The Open Aircraft Project is an initiative by the UK CASCADE Programme Grant team to create small unoccupied aerial system (SUAS) designs which are freely available to all. Starting with a representative but challenging set of mission requirements, two individual teams have designed, built and test flown competing vertical take-off and landing (VTOL) configurations. This paper describes the contribution made to this project by the University of Bristol. A tail-sitter configuration was explored in order to achieve launch and recovery within restricted spaces, and the wing design was chosen to achieve a compromise between low-speed, range and endurance objectives. The resulting aircraft show improved performance over existing designs that will be invaluable in facilitating volcanic survey flights at ranges and payloads greater than currently achievable. Results are given for both a scaled version and the final full size aircraft.

Nomenclature

UAV	=	Unoccupied aerial vehicle
$VTOL$	=	Vertical take-off and landing
$STOL$	=	Short take-off and landing
$AMSL$	=	Above mean sea level
$MTOM$	=	Maximum take-off mass
$MCTOM$	=	Maximum conventional take-off weight
$MVTOW$	=	Maximum vertical take-off weight
$CFRP$	=	Carbon fibre reinforced plastic
CG	=	Centre of gravity
S	=	Wing area
w	=	Wing span
c	=	Chord
MAC	=	Mean aerodynamic chord
AR	=	Aspect ratio
LE	=	Leading edge
e	=	Oswald span efficiency
ESC	=	Electronic speed controller
L	=	Overall Length
U	=	Airspeed
C_l	=	Lift coefficient
$C_{L_{max}}$	=	Maximum lift coefficient
C_d	=	Drag coefficient
C_{d0}	=	Zero lift drag coefficient
C_{dp}	=	Profile drag coefficient

*Research Associate, Department of Aerospace Engineering, University of Bristol
†UAV Technical Specialist, Department of Aerospace Engineering, University of Bristol
‡PhD Candidate, Department of Aerospace Engineering, University of Bristol
§PhD Candidate, Department of Aerospace Engineering, University of Bristol
¶Senior Lecturer, Department of Aerospace Engineering, University of Bristol
‖Senior Research Associate, Department of Aerospace Engineering, University of Bristol
**Undergraduate Student, Department of Aerospace Engineering, University of Bristol
††Senior Lecturer, Department of Aerospace Engineering, University of Bristol

η	=	Propulsive efficiency
P_{req}	=	Power required for steady level flight
V	=	Voltage
C	=	Capacity (A h)
Rt	=	Battery hour rating (h)
n	=	Discharge parameter

I. Introduction

The Complex Autonomous Aircraft Systems Configuration, Analysis, and Design Exploratory (CASCADE) began in 2018 as a collaborative research project among five of the UK's leading research institutions (the Universities of Southampton, Bristol, Cranfield, Manchester, and the Imperial College). CASCADE is a five-year program and is funded by the Engineering and Physical Sciences Research Council and by a growing network of industrial partners including NERC British Antarctic Survey, Consortiq, Thales, InMarSat, NATS, Boeing, BT, QinetiQ, and Network Rail, the U.K. Department for Transport, and the U.K. Civil Aviation Authority. The goal of CASCADE is to accelerate the exploitation of aerial robotics across a wide range of science and industry applications through fundamental research and practical demonstrations.

The Open Aircraft project is an initiative from CASCADE designed to meet the requirements of the science community when using small unoccupied aerial system (SUAS), fixed-wing drones in challenging remote locations. A set of design requirements have been created, primarily based on flight tests in Guatemala over Volcán de Fuego - but which meet the needs of a wide range of different science and industry challenges. The two teams currently involved - University of Southampton and the University of Bristol have committed to making all design details and test flight data freely available for download.

This paper describes the design of a Vertical Take-Off/Landing (VTOL) tail-sitter Unmanned Aerial Vehicle (UAV) for carrying and deploying scientific payloads. It goes on to describe the efforts made to establish the range and endurance capability of the platform. An image of the UAV discussed in this paper is shown in Figure 1.

The design is based on a list of requirements which envelop a range of possible scientific missions, often involving harsh environments which limit platform size and launch/recovery methods. The profiles and characteristics of these missions have been compiled from experience gained during extensive field work in such environments; the required performance cannot be achieved with any of the University of Bristol's existing fleet of UAVs or any commercially available UAV.

VTOL UAV operations are typically achieved using one of three configurations; tail-sitters [1, 2], tilt-rotors [3], and quad-planes [4, 5]. These configurations often involve carrying additional weight or adding drag in order to attain hovering/vertical flight. This often comes in the form of mechanisms, motors, or propellers, which become redundant in forward flight [6]. The tail-sitter configuration has been chosen here because the only notable concession in design and operation, compared to a conventional fixed wing of the same form, are the oversized motors. These are required in order to provide the additional thrust needed for hover, and may be made use of in forward flight in certain atmospheric conditions or at high altitude [7].

The range and endurance capability of a tail-sitter UAV can be improved by minimising the power required in the fixed wing and hovering conditions. Both of which can be improved by reducing overall weight, aerodynamic drag, and propulsive efficiency. Further mission performance gains can be achieved by ensuring the forward flight faces are performed at the optimum airspeed and by reducing the time spent hovering.

The risks associated with the design of such a large, relatively unconventional tail-sitter were mitigated by producing a smaller version quickly at the beginning of the project. This aircraft, named BUDDITA, is described in Section III. Extensive testing has been performed with BUDDITA, including successful VTOL operations and transitions to and from fixed wing flight. A video demonstrating these tests is presented here: https://www.youtube.com/watch?v=j5UBwVoKF3I. Performance tests performed with BUDDITA are described in Section IV.B, and compared to theorised performance in forward flight and hover. These results show a good correlation to the predicted forward flight performance, noting that C_{d0} and η must be generated empirically and used to calibrate the predictions.

The full size UAV, referred to as BUDDI (Bristol University Drone Design Initiative), is complete and awaiting test flights. The aircraft is described in Section II. The mission capability of BUDDI is discussed in Section V.

Fig. 1 Configuration Overview

A. Requirements Definition

Many scientific missions are envisaged such as volcanic ash collection [8], volcanic gas sensing [9], nuclear radiation mapping [10] and wildlife surveying. Scientific missions such as these are demanding due to a combination of performance and operational requirements, where heavy brush or rocky ground prevents conventional take-off and landing, whilst the necessary range and endurance cannot be achieved with a rotary wing UAV. The requirements given here are shared by the University of Bristol and the University of Southampton, and are primarily driven by the mission requirements for ash sampling over Volcán de Fuego in Guatemala. Volcán de Fuego is an active volcano with small explosions up to four times per hour and larger events every 6–8 weeks. The operational environment around Fuego is extreme; it is common for the aircraft to encounter strong winds at altitude, with high levels of atmospheric turbulence during missions to the summit region. In addition to highly variable wind, aircraft also experience large temperature variations and unpredictable, rapidly developing meteorological clouds. Current missions fly upwards of 10,000ft above take-off and spend up to 25 minutes at altitude collecting ash samples. The flight envelope that existing aircraft meet, in conjunction with the need for VTOL operations are given here:

- **Performance**
  - Service ceiling: 5000 m
  - Endurance: 30 min at altitude, 60 min at sea level
  - Cruise speed: minimum of 20 m/sec
- **Payload**
  - Mass: greater or equal to 0.8 kg
  - Minimum payload bay size: 180 x 150 x 100 mm
  - Quick release connections and easy access
- **Operational**
  - System must fit within the size limits for a single commercial hold bag: width + length + height $\leq$ 320 cm.
  - System is ideally under 23kg and must be under 32kg for transportation.
  - Power train must have a fully electric option
  - VTOL capability from 1100 m AMSL

II. BUDDI System Description

A. Structure

A diagram of BUDDI is shown in Figure 2. Key dimensions and parameters are listed in Table 1. A flying wing configuration is commonly chosen for tail-sitter UAVs, as it provides a lower center of mass when standing on the ground. A more conventional wing plus horizontal stabiliser layout was selected for this project for its improved handling in forward flight, to enable a wider CG range and to enable conventional and STOL operations. An additional benefit of a

conventional configuration is in the reduced risk associated with development and operations, as all phases of flight can be performed manually if necessary. The disadvantage of a conventional configuration is that when touching down vertically the aircraft must fall from a vertical orientation to a horizontal orientation, requiring an oversized landing gear to carry the additional load.

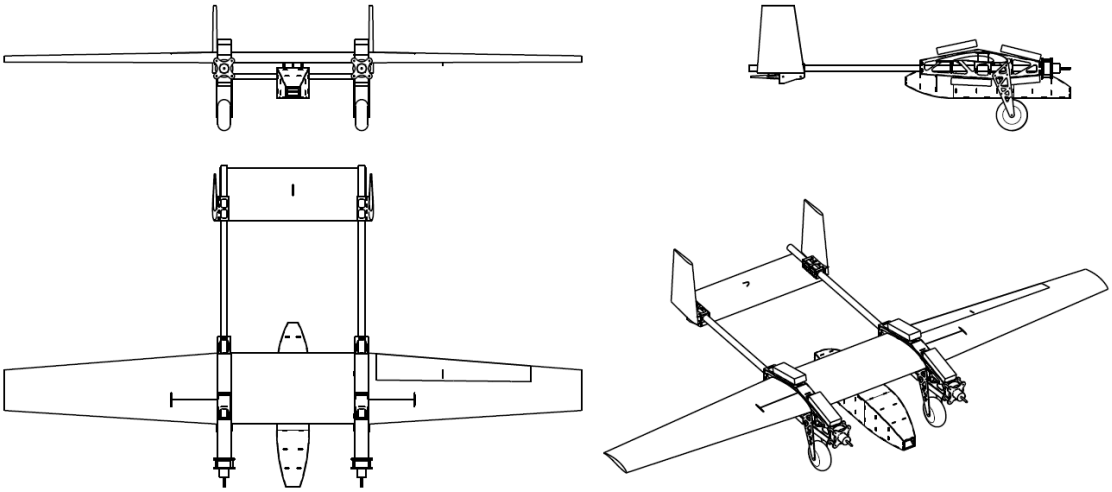

Fig. 2 BUDDI 3 View Drawing

The twin motor, twin boom configuration was chosen in order to separate the scientific payload from the propeller slip stream and to provide additional yaw authority, via differential thrust, in the hover condition. This configuration also provides operational benefits in that the scientific payload can be easily and completely separated from the avionic systems between flights.

The wings are constructed from hot-wire cut polystyrene cores laminated with 1.5 mm balsa wood sheeting. The payload bay and modular fuselage joints are built principally from laser cut birch plywood and balsa wood parts. The under-carriage and tail booms are built from $CFRP$ sheets and tubes respectively. These materials and construction methods are well established in the model aircraft hobby and produce an extremely light low cost structure.

Table 1 BUDDI key Parameters and Dimensions

Dimension	Value
w	2.6 m
S	0.79 m^2
L	1.300 m
MAC	0.320 m

Parameter	Value
$MVTOW$	11.0 kg
$MCTOW$	14.2 kg
AR	8
Wing Section	Wortmann FX 63-137

B. Avionics

The equipment selected for the UAV is listed in Table 2. The twin motor, tail-sitter configuration requires matching propellers with opposing directions of rotation. The availability of reverse rotation propellers in this size range is limited so much of the sizing was constrained around these.

The batteries selected are some of the highest energy density lithium polymer sells available on the hobby market. Other technologies, such as lithium-ion, can have higher energy densities but are unable to produce the peak current required for hovering flight. Two battery configurations are specified. The 2S 2P arrangement allows VTOL operations and the 2S 4P arrangement allows a longer mission where STOL and conventional operations are possible. Each individual battery is less than 160 W h so it can be carried as hand luggage on commercial passenger flights.

The selected Flight Control Module (FCM) is a well respected unit with tripple IMU's and internal vibration damping. The form-factor is compact giving the freedom to locate the unit inside the main wing. Arudpilot was selected

as the flight control software as it allows for in-flight switching between conventional aeroplane flight mode into tail sitter flight mode. Specific parameters and tuning values can be applied to each mode allowing greater control. The current stable release (4.0.3) supports the majority of what is required. Additional functionality can be added into the code base or via LUA scripting.

The FCM communicates with the ground station via the telemetry data link to enable real time monitoring during flight as well as to enable configuration changes on the fly.

Table 2 List of avionic systems selected for BUDDI

Item	Description
Motor (x2)	AXI8118-10
Propeller	APC 21x13E and APC 21x13EP
Electronic Speed Controller (x2)	D3 Motors F3A ESC
Actuators	7 digital servos
Lithium Polymer Batteries, VTOL Operations	4 x Overlander 5S 8000 mA h (2S 2P Configuration)
Lithium Polymer Batteries, STOL Operations	8 x Overlander 5S 8000 mA h (2S 4P Configuration)
Flight Control Module	Hex - Cube Black
Flight controller Software	ArduPlane 4.0.1
Power Monitoring	Mauch 14S current and voltage
Telemetry Data Link	RFD868+

C. Sizing and performance

The size of the UAV was selected based on performance estimations for a wing span range from 2.2 m to 3.2 m, at airspeeds of 20 m/sec and 25 m/sec, sea level and 5000 m $AMSL$. For a given airspeed this prediction is based on the predicted drag force, the propulsive efficiency and the effective battery capacity using the method defined in [11]. The mass was estimated based on a list of materials and parts and an estimated baseline mass for each item. The mass of each item was then either defined as a constant, for items such as the installed equipment, or scaled with with w (weight), S (wing area) or w^3, depending on the nature of the part. For example, the mass of the polystyrene wing core material is scaled with w^3, whereas the mass of the balsa wood wing sheeting is scaled with S. Figure 3 shows the estimated mass and stall speed for a range of w. Stall speed was estimated based on a $C_{L_{max}}$ of 1.3, taking a conservative interpretation of UIUC low speed data and allowing for a reduction due to three-dimensional effects. An additional assessment was performed with a contingency mass of 4 kg. This contingency estimation was considered in the sizing process to reduce the risk of the original weight estimate being overly optimistic.

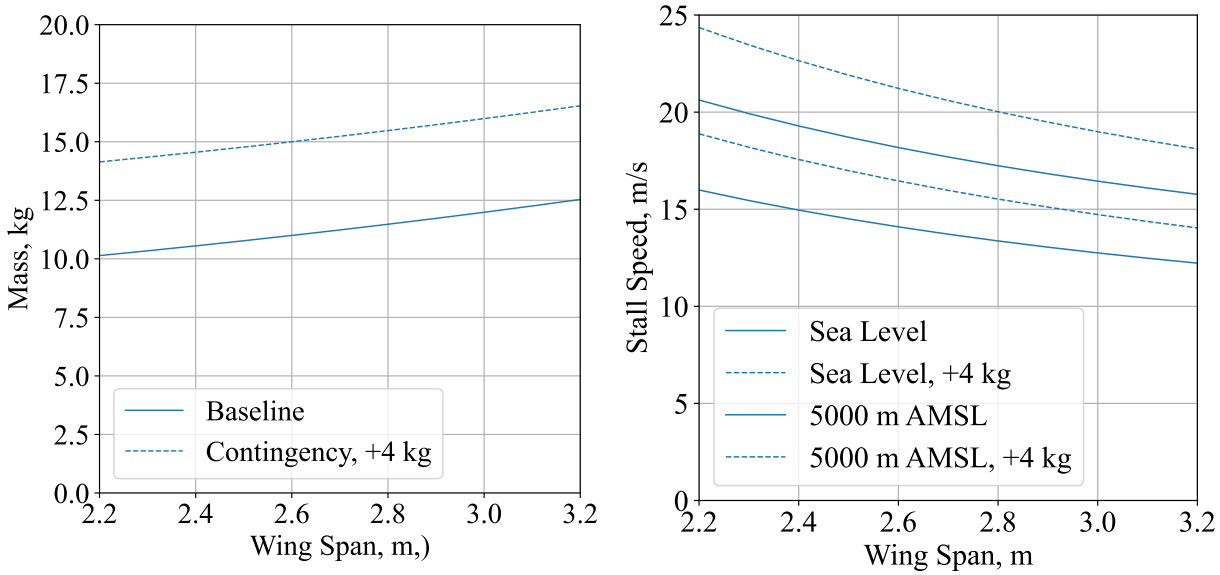

Fig. 3 Mass and stall speed estimates for a range of wing spans

Range and endurance are found using the known battery capacity, propulsive efficiency and power required for steady level flight, given as

$$P_{req} = \frac{1}{2}\rho U^3 S(C_{D_0} + kC_L^2) \tag{1}$$

where C_L is constant and will normally correspond to either a maximum range or endurance condition. Endurance may then be found using the total battery capacity available, reduced according to the Peukert effect as

$$t_{endurance} = \left(\frac{\eta VC}{P_{req}}\right)^n R_t^{1-n} \tag{2}$$

In these results k is calculated assuming an elliptic lift distribution and a mid-semi-span 2D quadratic profile drag calculated using Xfoil. C_{D_0} is taken as 0.03 based the performance calibration performed with BUDDITA, described in Section IV.B. The propulsive efficiency, η is split in to two components, η_{prop}, to account for the losses attributed to the propeller, and η_{motor} to account for the losses attributed to the motor and ESC. The propeller manufacturer produces performance data for its propellers which is generated using the NASA Transonic Airfoil Analysis Code, [12]. This data provides propulsive efficiency for a range of air speeds and thrusts. η_{prop} is linearly interpolated from this data. η_{motor} is taken as 0.325 based on the performance testing in Section IV.B.

$$\eta = \eta_{prop}(Thrust, U)\eta_{motor} \tag{3}$$

To find final performance in either the maximum range or endurance cases, the optimal C_L for either condition is substituted to find the corresponding value of P_{req}, which then gives the endurance. The range may then be found by multiplying this time by the speed that corresponds to the chosen C_L condition.

To find these C_L conditions an energy argument implies that to maximise range, where the work done W is $D \times S$, drag D should be minimised, subject to $C_L V^2 = const.$ to maintain equilibrium. This implies the drag is proportional to $C_D V^2 = const.\frac{C_D}{C_L}$, requiring operation at best L/D, for which the lift coefficient is

$$C_{L_{range}} = \sqrt{\frac{C_{D_0}}{k}} \tag{4}$$

Maximising endurance instead requires a minimum in power, given by $D \times V$, where V is proportional to $\frac{1}{\sqrt{C_L}}$ and the power is $D \times V^3$, leading to a requirement to minimise $\frac{C_D}{C_L^{\frac{3}{2}}}$, which gives

$$C_{L_{endurance}} = \sqrt{\frac{3C_{D_0}}{k}} \tag{5}$$

The conclusion of this is that best endurance requires a lift coefficient greater by a factor of $\sqrt{3} = 1.73$, and hence a preference to select an aerofoil/wing that can reach this value before stalling. For an aspect ratio of around 8, with $C_{D_0} = 0.03$ (which estimates total lift-independent drag) and $k = 0.0476$ (which includes only wing induced drag plus a parabolic 2D profile drag), this gives

$$\frac{W}{S} = \sqrt{\frac{0.03}{0.0476}} \frac{1}{2} 1.225 \times 20^2 = 19.8 \frac{g}{m^2} \tag{6}$$

ie. 19.8kg/m^2. It is notable that the requirement for good range at 20m/s, which is dictated by the prevalence of strong winds at cruise altitude, effectively sets the wing area. Ordinarily, a lower loading with higher aspect ratio would improve range, but it would do so at a speed that would no longer make effective progress against the likely headwinds.

Aerofoil selection trades several considerations against each other. Best endurance requires low speeds and quite high C_L values, so it is preferable to have a good $C_{L_{max}}$ to ensure that the best endurance condition preserves some margin to stall. If $C_{L_{max}}$ is compromised, the best endurance condition may become unreasonably close to stall, or may not even be achievable. For landing and low-speed flight, retaining good $C_{L_{max}}$ is also beneficial, so it is an important parameter to retain.

Alongside $C_{L_{max}}$ achieving good L/D requires a low C_{D_0}, and these two parameters generally show a shadowing trend with low drag also associated with low maximum lift. For structural behaviour, thicker sections are preferable as they provide improved second moment of area, offering the opportunity for improved stiffness at fixed weight or lower weight for fixed stiffness, as well as greater battery volume.

With wing area fixed, aspect ratio and taper/twist remain to be chosen. In order to minimise induced drag, taper ratio and twist are determined in order to approximate an elliptical spanload, with the caveat that the centre section is not tapered in order to preserve volume and chord for housing aircraft systems, such that taper can conveniently begin outboard of the motors. This also fits comfortably alongside the concept of swapping outboard wing panels to change wing area for differing missions.

Selection of aspect ratio is a tradeoff between reducing induced drag and avoiding awkwardly small chord lengths and Reynolds numbers. Below a Re of 100,000 many sections begin to show anomalous stall, drag and moment behaviour, as well as a general increase in section C_{D_0}. Effectively, this precludes very narrow chords, even before the weight considerations of high aspect ratio are included. Furthermore, the reciprocal relation of induced drag with aspect ratio means the most worthwhile improvements are of course for the initial increases in aspect ratio.

Aerofoil philosophy for BUDDI is therefore not to aim for low C_{D_0} (because the rest of the aircraft already adds considerable drag) or the very best L/D, but to retain thickness and $C_{L_{max}}$ without incurring an excessive C_{D_0} penalty. It is also important to have acceptable drag behaviour over a good C_L range, rather than at a very restrictive C_L. Payloads for BUDDI are necessarily unknown and there needs to be flexibility in the choice of operating point for a particular mission based on weight and prevailing wind conditions.

It is perhaps not surprising that the design of small aircraft is linked closely to wind conditions, especially at the target altitudes used here. Nonetheless, the design can be readily adapted to increase area for a mission that may involve more loitering or no vertical takeoff, and there is considerable scope to adjust the wide-chord wide-span flaperons over the course of a flight.

Endurance and range predictions are shown in Figure 4. The graphs show that at sea level both range and endurance can be maximised by selecting the smallest wing span option. At altitude and especially when the contingency is included in the mass prediction the benefits of a wing span in the 2.4 m to 2.8 m range become more clear. This is reinforced by consideration of the stall speeds in Figure 3.

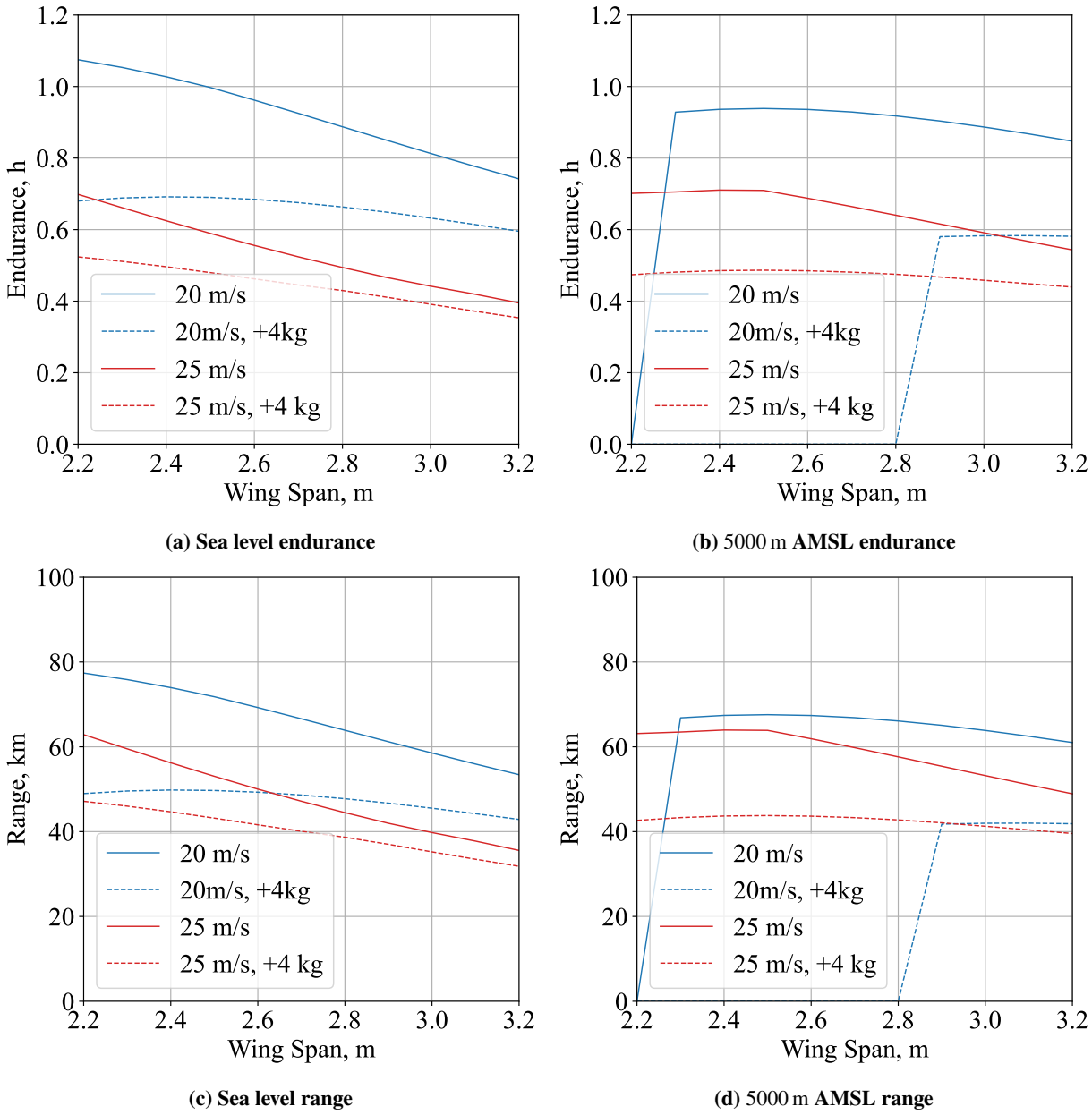

(a) Sea level endurance

(b) 5000 m **AMSL endurance**

(c) Sea level range

(d) 5000 m **AMSL range**

Fig. 4 Forward flight performance predictions for a range of wing spans

III. BUDDITA System Description

Key parameters for BUDDITA are listed in Table 3 and the equipment used is listed in Table 4

Table 3 BUDDITA key dimensions and parameters

Dimension	Value
w	1.68 m
S	0.32 m^2
L	1.00 m
MAC	0.20 m

Parameter	Value
$MTOW$	3.23 kg
AR	8
Wing Section	NACA 2411

Table 4 List of avionic systems selected for BUDDI

Item	Description
Motor (x2)	AXI2826/13
Propeller	APC 12x6E and APC 12x6EP or APC 12x8E and APC 12x8EP
Electronic Speed Controller (x2)	JETI Spin 66
Actuators	5 digital servos
Lithium Polymer Batteries (x2)	Overlander 6S 4000 mA h (2P Configuration)
Flight Control Module	Pixhawk Pixracer
Flight controller Software	ArduPlane 4.0.1

IV. Calibration of Performance Predictions

A. Hover performance Calibration

In order to establish the power needed to hover average voltage and current readings were taken over set of performance tests performed with buddita. Figure 5 shows one of these tests in progress.

Fig. 5 Hover performance testing

The hover power is calculated from flight data and compared to the predicted power needed to produce the required thrust from manufacturers propeller data. The difference between the measured power and the predicted power from the propeller data is attributed to losses in the motor and speed controller. Figure 6 shows the propeller manufacturers performance data for zero airspeed. The point representing the average measured power during hover is plotted, along with the predicted power based on linear interpolation, showing that the ratio of predicted hover power to measured hover power is 0.88.

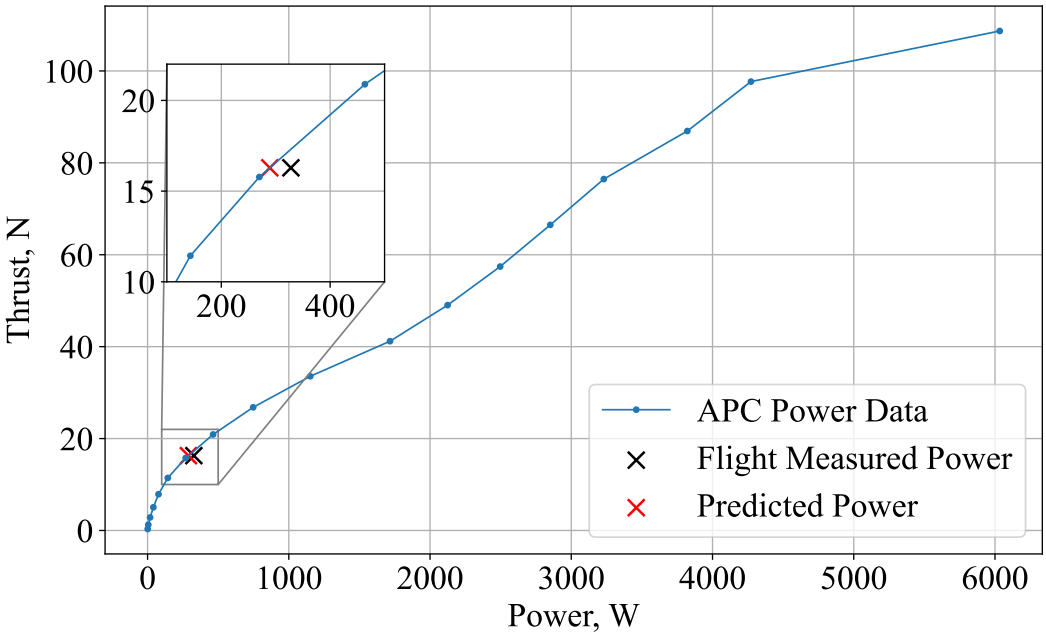

Fig. 6 Power required to hover

For initial design calculations the power required to hover is calculated according to

$$P_{hover} = 2P_{prop}(0.5Mg)/0.88 \tag{7}$$

Where the function P_{prop} is a linear interpolation on the propeller manufacturers data at zero airspeed. The required thrust per motor, P_{hover} and the corresponding hover endurance calculated according to Equation 2 are shown in Table 5. This calculation demonstrates that the STOL version of BUDDI does not have the power required to hover, as P_{hover} is greater than the maximum power rating of the two motors combined (5600 W) This result needs to be validated by test as the performance data is unreliable at low airspeed.

Table 5 BUDDI hover performance

Version	VTOL	STOL
Required Thrust per motor	53.96 N	73.57 N
P_{hover}	4444 W	7080 W
Hover Endurance	4.75 min	2.53 min

B. Forward Flight Performance Calibration

Forward flight performance tests were performed with BUDDITA in order to calibrate the predictions described in Section II.C. The tests comprised repeating rectangular circuits whilst attempting to maintain a range of different air speeds. Tests were performed with the two sets of propellers listed for BUDDITA in Section III. Calibration is performed in order to establish C_{D_0} and any additional contributions to the propulsive efficiency, η on top of that already accounted for in the propeller.

Limitations at the test location necessitated the relatively small circuit, which caused continuous variations in airspeed, altitude, lift force, forward acceleration, roll angle and control surface deflections. In order to account for these variations the measured power at each time step was compared to a predicted power based on the state of the aircraft at that time step.

$$P_{prediction} = T_{req} * U/\eta \tag{8}$$

The required thrust, T_{req} is calculated based on the instantaneous airspeed, load factor and forward acceleration. These values are calculated by the FCM and logged during the performance test.

$$Thrust = qS(C_{D_0} + k(\frac{A_z M}{qS})^2) + MA_x \tag{9}$$

$$q = \frac{1}{2}\rho U^2 \tag{10}$$

The measured power at each time step is calculated from logged voltage and current data. Sensor data is only available from one motor, so the assumption is made that both motors are performing similarly.

$$P_{measured} = VA * 2 \tag{11}$$

Figure 7 shows an extract of the comparison produced using the above approach around one corner and the following straight leg. Figure 7a shows the variations in altitude, airspeed, measured power and predicted power against time. Figure 7b shows the trace of the aircraft position in the horizontal plane, which was followed in the anti clockwise direction. The graphs show that the airspeed increases through the turn, then reduces again in the straight section. This is coupled with a slight loss of height through the turn and corresponding recovery afterwards. This behaviour is attributed to the FCMs total energy control system and could be improved with further tuning of the turn settings at this airspeed.

The measured power in Figure 7a increases sharply at the start of the turn, then remains high throughout the turn and reduces on the straight leg. The predicted power follows the behaviour well at the start of the turn and on the straight leg, but drops off more quickly than the measured power through the turn. This may be attributed to factors which are not accounted for in the simple model such as the increased drag due to control surface deflections or some local separation due the the high C_L through the turn. Note a low pass filter has been applied to smooth the data presented in Figure 7a.

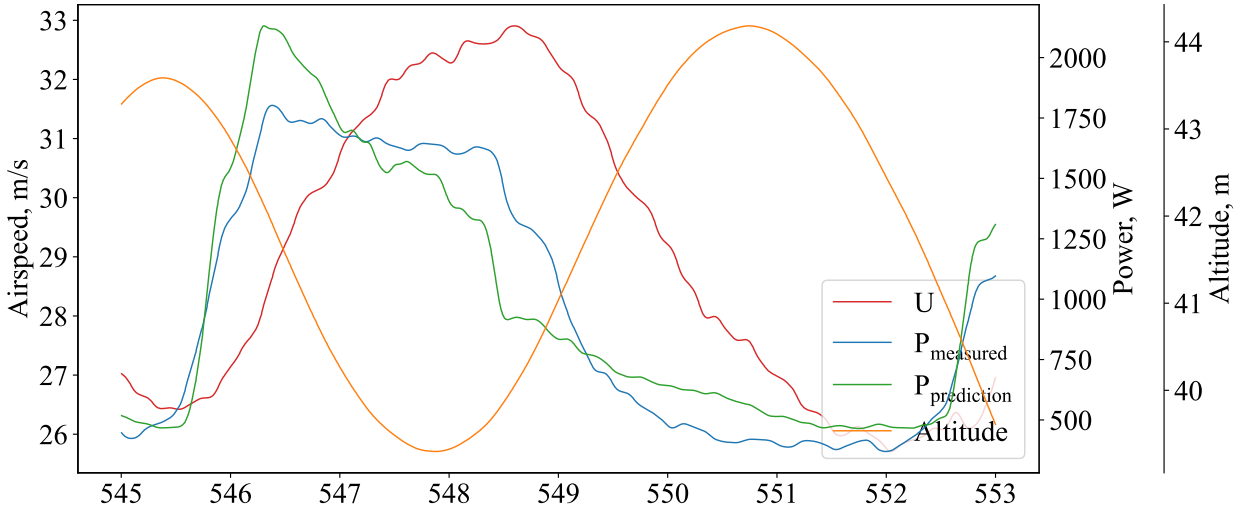

(a) Airspeed, measured power and predicted power against time

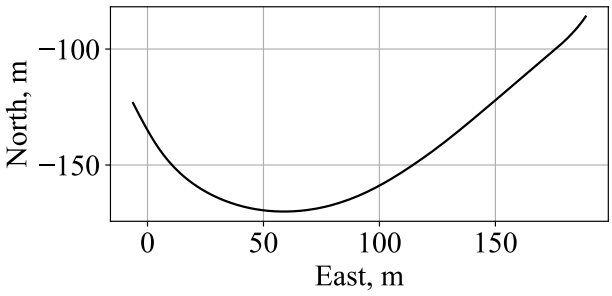

(b) xy trace

Fig. 7 Extract of BUDDITA performance test time history

The scientific missions envisaged comprise long, straight sections and only occasional turns. The poor fit of the measured power to the predicted power through turns is therefore considered acceptable for the purpose of this study. Figure 8 shows averages of the measured and predicted power consumption within each airspeed region of the performance tests with the two prop combinations. The averages are produced only from the data where the roll angle is within 10 deg of level. The lines in Figure 8 show the predicted power consumption for BUDDITA in straight and level flight for the range of airspeeds. In order to produce this graph C_{D_0} was set to 0.03 and the factor η_{motor} set to 0.325 to account for losses in the motor and speed controller.

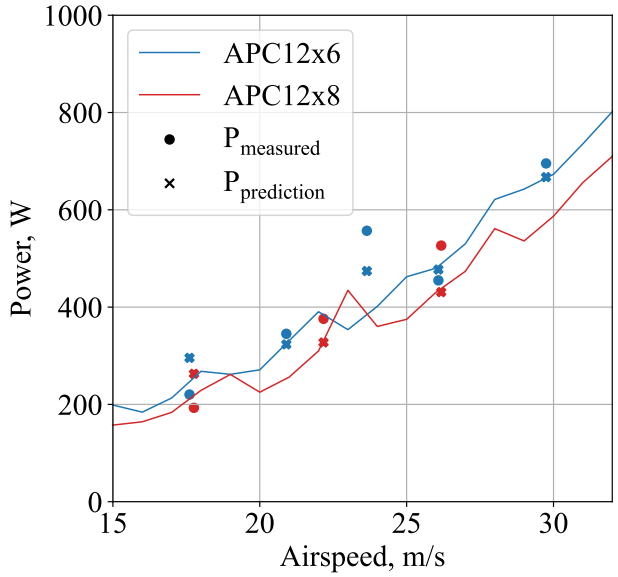

Fig. 8 Interpreted results of BUDDITA performance testing

V. BUDDI Mission Profile

The capability of BUDDI cannot be quantified entirely by considering the range and endurance estimations for forward flight, as the additional energy used during takeoff, climb and landing must also be considered. The sea level STOL graph may be considered representative as conventional takeoffs and landings contribute only a small proportion of the total mission energy usage. A similar assumption is made about vertical takeoffs and the subsequent transition to forward flight, as well as the transition from forward flight to hover before landing. Whilst these maneuvers demand a high peak power output, they last only a short time and therefore little energy is used.

The time spent hovering prior to landing contributes a significant proportion of the total mission energy usage. The transition from forward flight to hover must finish at a relatively high altitude and vertical descent rates are limited to around 0.5 m s^{-1}. Figure 9 shows a visualisation of a transition from forward flight to hover. The transition is controlled by the FCM and is a typical example of those performed with BUDDITA. The figure demonstrates that the manoeuvre was completed with an altitude gain of around 13 m. This altitude gain must be considered on top of the minimum safe altitude at which a UAV can be autonomously flown, of around 20 m, when ground based obstacles and barometric drift are considered. This equates to a total time spent hovering prior to landing of 66 s. Scaling the total hover endurance calculated in Table 5 gives a conservative estimate for the proportion of the total available battery that will be used in this portion of flight of 23 %.

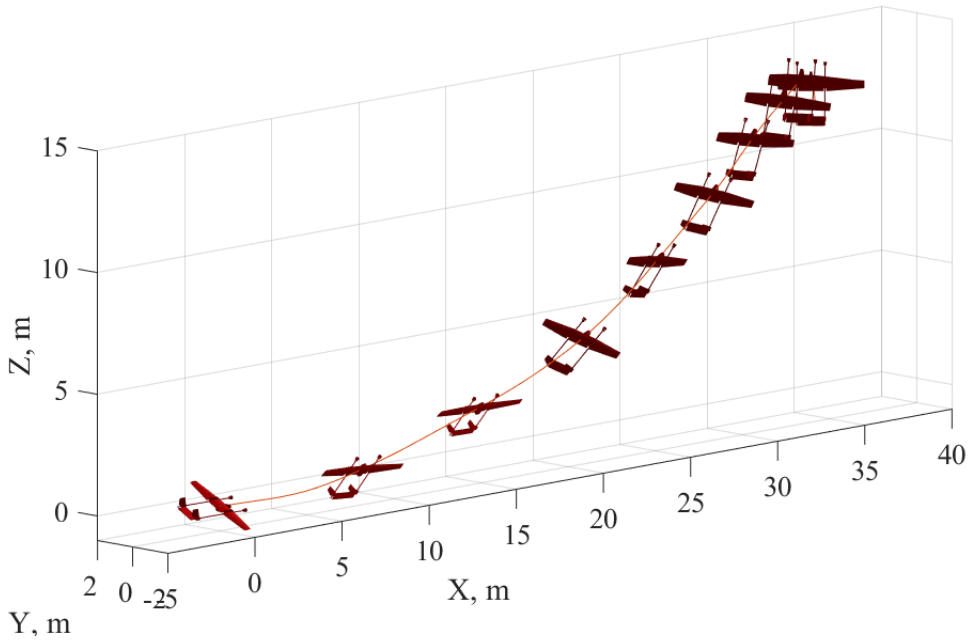

Fig. 9 Auto transition

Figure 10 shows a typical example of a transition performed with BUDDITA by a human pilot. It demonstrates that it is possible to complete the transition with a smaller altitude gain (around 8 m in this case) than that achieved by the FCM. It is also possible to begin a manual transition at a much lower altitude as the human pilot has a visual reference for the height of the ground and any obstacles. In the highlighted example the transition began at an altitude of 2 m. The total hover descent of 10 m after a manual transition reduces the proportion of battery used for the vertical landing to 7 %.

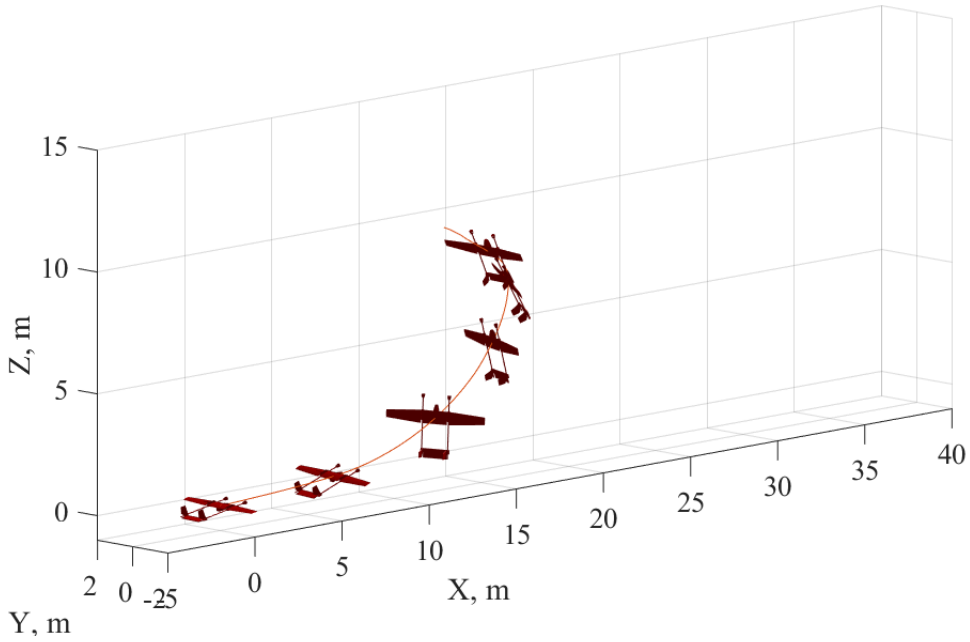

Fig. 10 Manual transition

Requiring human pilots for segments of otherwise autonomous missions is not desirable, and future work will consider means of completing the transition from fixed wing to hover at low altitude with less human input. These may

include additional sensors to better detect ground obstacles and barometric drift, tuning of the transition controller for minimum altitude gain, or considering different transition maneuvers such as the integration of a snap roll.

Revised mission capability predictions for BUDDI are presented in Figure 11, with the total battery capacity available reduced by 15 % and 5 % respectively to account for the energy used during takeoff and landing.

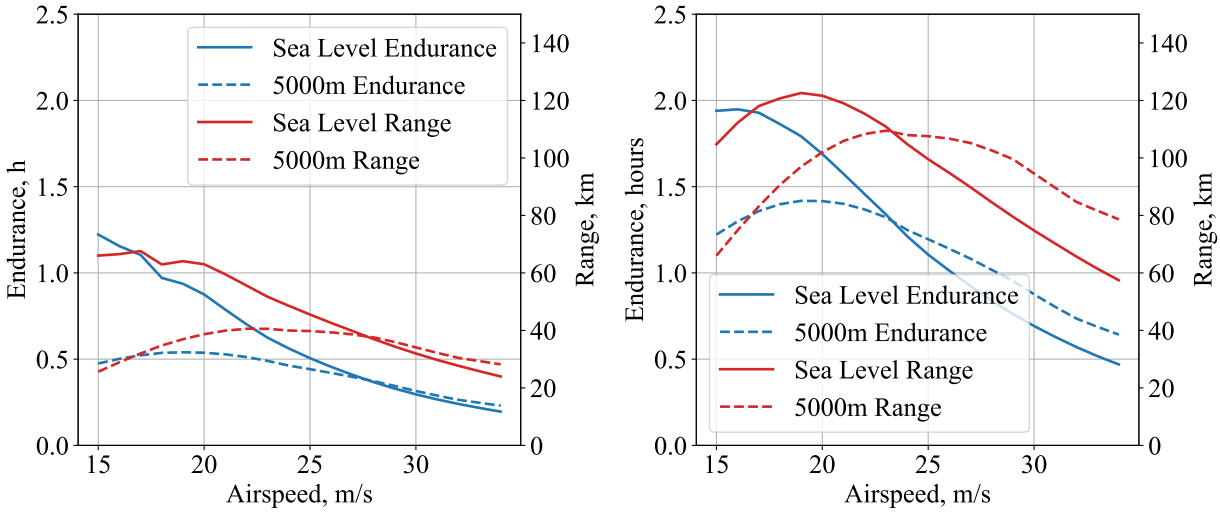

(a) VTOL Operations **(b) STOL Operations**

Fig. 11 BUDDI range and endurance

In order to establish whether BUDDI will be capable of performing the volcanic ash sensing mission described in Section I.A the method described in Section IV.B was applied to a flight log of the actual mission performed by a Skywalker X8 UAV. A rolling integral of the predicted power required for BUDDI was calculated to give the total predicted energy used throughout the flight.

The assessment is presented in Figure 12, with the orange and blue lines representing logged altitude and airspeed respectively. The red lines show the percentage of the available capacity used against time. The assessment suggests that the mission can be completed by the STOL version of BUDDI, as the consumption remains below 100 % at the end of the mission. The graph also shows that the VTOL version of BUDDI would run out of battery somewhere near the top of the ascent. This simulation is overly pessimistic as the optimum mission profile selected for BUDDI would not match that used in the log. For example the X8 has a higher lift to drag ratio than BUDDI and as such the un-powered descent for the skywalker requires some thrust for BUDDI to maintain the same glide angle and airspeed. If the mission were performed with BUDDI a higher descent rate and lower airspeed would be selected and the energy used during the descent would be effectively zero.

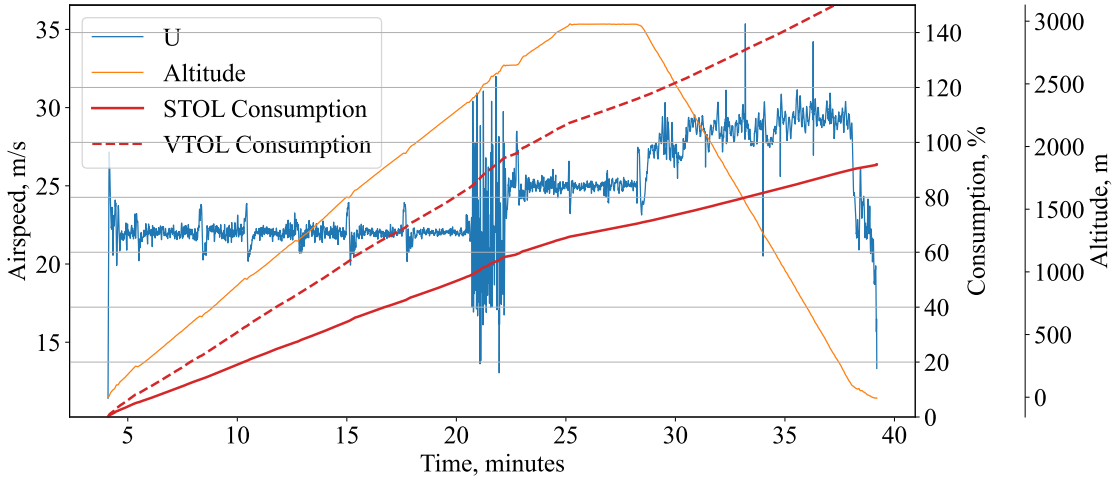

Fig. 12 Simulation of volcanic ash collection mission with BUDDI

VI. Conclusion

This paper discussed the design and development of a portable UAV for the high-performance requirements of a volcanic survey mission. Two mass options are described, the lighter allowing VTOL operations and the heavier for extended range and endurance STOL operations. Methods for predicting the performance in hover and forward flight were set out and calibrated using a scaled-down demonstrator version of the UAV. The approach improves the range and endurance of a tail-sitter by predicting optimum speed during forward-flight and minimising hover time. Simulation of two configurations against a recorded mission profile shows that the STOL configuration can achieve the mission, carrying a 1 kg scientific payload to the top of Volcán de Fuego in Guatemala. Further testing is required to see if the mission can be achieved with the VTOL configuration, but the design already offers significant benefits to volcanic research. Future work includes the integration of more sensors to reduce the transition height with less pilot input.

Acknowledgements

This work was supported by the Engineering and Physical Sciences Research Council through the CASCADE Programme Grant, reference EP/R009953/1.

References

[1] De Wagter, C., Ruijsink, R., Smeur, E. J., van Hecke, K. G., van Tienen, F., van der Horst, E., and Remes, B. D., "Design, control, and visual navigation of the DelftaCopter VTOL tail-sitter UAV," *Journal of Field Robotics*, Vol. 35, No. 6, 2018, pp. 937–960. https://doi.org/10.1002/rob.21789.

[2] Verling, S., Weibel, B., Boosfeld, M., Alexis, K., Burri, M., and Siegwart, R., "Full Attitude Control of a VTOL tailsitter UAV," *Proceedings - IEEE International Conference on Robotics and Automation*, Vol. 2016-June, 2016, pp. 3006–3012. https://doi.org/10.1109/ICRA.2016.7487466.

[3] Yuksek, B., Vuruskan, A., Ozdemir, U., Yukselen, M. A., and Inalhan, G., "Transition Flight Modeling of a Fixed-Wing VTOL UAV," *Journal of Intelligent and Robotic Systems: Theory and Applications*, Vol. 84, No. 1-4, 2016, pp. 83–105. https://doi.org/10.1007/s10846-015-0325-9, URL http://dx.doi.org/10.1007/s10846-015-0325-9.

[4] Orbea, D., Moposita, J., Aguilar, W. G., Paredes, M., Reyes, R. P., and Montoya, L., "Vertical take off and landing with fixed rotor," *2017 CHILEAN Conference on Electrical, Electronics Engineering, Information and Communication Technologies, CHILECON 2017 - Proceedings*, Vol. 2017-Janua, 2017, pp. 1–6. https://doi.org/10.1109/CHILECON.2017.8229691.

[5] Yu, S., and Kwon, Y., "Development of VTOL Drone for Stable Transit Flight," *Journal of Computer and Communications*, Vol. 05, No. 07, 2017, pp. 36–43. https://doi.org/10.4236/jcc.2017.57004.

[6] Serrano, A. R., "Design methodology for hybrid (VTOL + Fixed Wing) unmanned aerial vehicles," *Aeronautics and Aerospace Open Access Journal*, Vol. 2, No. 3, 2018, pp. 165–176. https://doi.org/10.15406/aaoaj.2018.02.00047.

[7] Paredes, J. A., Saito, C., Abarca, M., and Cuellar, F., "Study of effects of high-altitude environments on Multicopter and Fixed-Wing UAVs ' Energy Consumption and Flight Time," *2017 13th IEEE Conference on Automation Science and Engineering (CASE)*, 2017, pp. 1645–1650.

[8] Schellenberg, B., Richardson, T., Watson, M., Greatwood, C., Clarke, R., Thomas, R., Wood, K., Freer, J., Thomas, H., Liu, E., Salama, F., and Chigna, G., "Remote sensing and identification of volcanic plumes using fixed-wing UAVs over Volcán de Fuego, Guatemala," *Journal of Field Robotics*, Vol. 36, No. 7, 2019, pp. 1192–1211. https://doi.org/10.1002/rob.21896.

[9] Liu, E. J., Wood, K., Mason, E., Edmonds, M., Aiuppa, A., Giudice, G., Bitetto, M., Francofonte, V., Burrow, S., Richardson, T., Watson, M., Pering, T. D., Wilkes, T. C., McGonigle, A. J., Velasquez, G., Melgarejo, C., and Bucarey, C., "Dynamics of Outgassing and Plume Transport Revealed by Proximal Unmanned Aerial System (UAS) Measurements at Volcán Villarrica, Chile," *Geochemistry, Geophysics, Geosystems*, Vol. 20, No. 2, 2019, pp. 730–750. https://doi.org/10.1029/2018GC007692.

[10] Connor, D. T., Wood, K., Martin, P. G., Goren, S., Megson-Smith, D., Verbelen, Y., Chyzhevskyi, I., Kirieiev, S., Smith, N. T., Richardson, T., and Scott, T. B., "Corrigendum: Radiological Mapping of Post-Disaster Nuclear Environments Using Fixed-Wing Unmanned Aerial Systems: A Study From Chornobyl (Frontiers in Robotics and AI, (2020), 6, (149), 10.3389/frobt.2019.00149)," *Frontiers in Robotics and AI*, Vol. 7, No. February, 2020, pp. 28–30. https://doi.org/10.3389/frobt.2020.00030.

[11] Traub, L. W., "Range and endurance estimates for battery-powered aircraft," *Journal of Aircraft*, Vol. 48, No. 2, 2011, pp. 703–707. https://doi.org/10.2514/1.C031027.

[12] Dougherty, F. C., Hoist, T. L., Gundy, K. L., and Thomas, S. D., "TAIR - a Transonic Airfoil Analysis Computer Code," Tech. rep., NASA, 2020.